Petroleum Science 23 (2026) 4927–4938

Contents lists available at ScienceDirect

Petroleum Science

journal homepage: www.keaipublishing.com/en/journals/petroleum-science

Original Paper

Numerical simulation of integrated “fracturing-soaking-production” in tight reservoirs

Li Ma [a,b,c], Jian-Chun Guo [b,*], Cong Lu [b,**], Shi-Qian Xu [b], Yi Song [a,c], Cheng Shen [a,c], Jun-Feng Li [a,c]

[a] *Shale Gas Research Institute, PetroChina Southwest Oil & Gasfield Company, Chengdu, 610051, Sichuan, China*
[b] *State Key Laboratory of Oil and Gas Reservoir Geology and Exploitation, Southwest Petroleum University, Chengdu, 610500, Sichuan, China*
[c] *Sichuan Key Laboratory for Shale Gas Geological Evaluation and Efficient Development, Chengdu, 610051, Sichuan, China*

A R T I C L E I N F O

Article history:
Received 6 March 2025
Received in revised form
24 December 2025
Accepted 2 March 2026
Available online 12 March 2026

Edited by Meng-Jiao Zhou

Keywords:
Tight reservoir
Fracturing-flooding technology
Hydraulic fracture
Imbibition displacement
Surfactant flooding
Numerical simulation

A B S T R A C T

Integrated fracturing-flooding is a key technology to solve the problem of “difficult injection and difficult extraction” in tight oil and gas reservoirs. Focusing on three key physical processes in the fracturing-flooding development of tight reservoirs: fracture propagation during water injection, imbibition displacement during well soaking, and oil recovery during production, taking into account the impacts of osmotic pressure and flooding agents, and integrating continuous damage theory, a mathematical model for fracturing flooding coupling hydro-mechanical-damage (H-M-D) in tight reservoirs was established. Furthermore, numerical simulations of the integrated “fracturing-soaking-production” process were conducted to clarify the impacts of geological parameters and fracturing-flooding engineering parameters on the development effects. The study shows that when matrix permeability is low, the formation's water absorption capacity is weak, and the rock damage degree is high, resulting in the formation of “long and narrow” fracture networks. As matrix permeability increases, the rock damage degree decreases, leading to the formation of “short and wide” fracture networks. The density of natural fractures affects the direction and distance of hydraulic fracture propagation. As the injection volume increases, the length of the fracture network increases, and the overall water absorption capacity of the fracture network improves, making it easier for the fractures to extend in the direction of stress dominance. During the soaking process, formation pressure diffuses, and under the influence of imbibition, the oil phase gradually migrates toward the fractures. Based on the research findings, an integrated “fracturing-soaking-production” stimulation engineering parameter optimization technique was developed, and an optimization chart for stimulation engineering parameters was established. Taking the fracturing-flooding case of the tight reservoirs in eastern China as an example, the optimized injection volume within a single layer for fracturing flooding ranges from 3×10^4 m^3 to 3.5×10^4 m^3, with injection rates ranging from 1000 m^3/d to 1200 m^3/d and a soaking duration of 20–30 days, and the development effects of the reservoirs with fracturing flooding are much better than that without fracturing flooding.

1. Introduction

In response to the challenges of “injection difficulties and low recovery” in low-permeability reservoirs, oilfields proposed the integrated “fracturing-soaking-production” fracturing-flooding technology in recent years (Guo et al., 2022; Cui et al., 2023a, 2023b; Cai et al., 2023). This technology involves injecting water at near-fracture pressures to create microfractures, expanding the swept volume, continuously injecting at high pressure to increase pore throat size and improve flow pathways, while also

* Corresponding author.
** Corresponding author.
E-mail addresses: guojianchun@vip.163.com (J.-C. Guo), lucong@swpu.edu.cn (C. Lu).

Peer review under the responsibility of China University of Petroleum (Beijing).

https://doi.org/10.1016/j.petsci.2026.03.002

replenishing reservoir energy. Subsequently, through well soaking imbibition, oil and water displace each other, enhancing oil recovery efficiency. Finally, combining chemical flooding, oil washing efficiency can be further enhanced. In recent years, the fracturing-flooding process has rapidly developed and been applied in low-permeability blocks in Daqing Oilfield, Changqing Oilfield, Jilin Oilfield, Tuha Oilfield, Huabei Oilfield, and Shengli Oilfield, achieving certain preliminary results, including a significant increase in water injection capacity and a noticeable improvement in productivity. However, a series of field issues have also emerged during the implementation of fracturing flooding in oilfields (Yang et al., 2023), such as the significant response direction on oil wells, rapid water cut increase, and quick production decline. The root cause of these issues is that the fracturing-flooding technology for low-permeability reservoirs is still in its initial stages of implementation. There is insufficient theoretical support, unclear mechanisms, and poorly understood influencing factors. Most engineering parameters are drawn from field experiences of conventional water injection and hydraulic fracturing, and the fracturing-flooding parameters are largely optimized and adjusted during implementation. Therefore, it is urgently necessary to conduct integrated fracturing-flooding theoretical research to identify the key controlling factors and to provide theoretical support for efficient on-site implementation.

One of the main mechanisms of fracturing flooding is to inject water at a near-fracture pressure, first proposed by Collins (2007). This method involves controlling the injection rate and pressure to inject fluid into the formation, generating microfractures near the wellbore, thereby improving the water absorption capacity of reservoirs (Ma et al., 2023). After the 21st century, many scholars began to study the hydraulic fracture propagation mechanisms by investigating the fracture tip failure mechanisms during water injection (Azeemuddin et al., 2002; Hustedt and Snippe, 2010; Wang et al., 2015; Zhou, 2017). Wang et al. (2019) analyzed water injection development in low-permeability reservoirs in Changqing Oilfield and found that even under conditions below fracture pressure, water injection could activate natural fractures, forming water injection fractures. These fractures can improve the injection capacity of low-permeability reservoirs but may also increase the risk of water coning in oil wells. The theorical imbibition model has evolved from analytical models to numerical models (Zhmud et al., 2000; Li and Horne, 2001; Amico and Lekakou, 2004; Ahrenholz et al., 2008; Li and Zhao, 2012; Hu et al., 2015; Wang et al., 2015), particularly with substantial theoretical research and field practice on water huff and puff in low-permeability reservoirs in recent years (Gao et al., 2018; Shen et al., 2018; Li et al., 2022; Shi et al., 2022; Xu et al., 2023). However, current imbibition models mainly focus on the reverse imbibition process of single-well water huff and puff. For the oil-water imbibition model under fracturing-flooding conditions with large-scale long-term well soaking, the effects of osmotic pressure caused by the difference in salinity between the injected water and formation water must be considered. Currently, there is a lack of theoretical research on this aspect, both domestically and internationally, which hampers the effective theoretical guidance for optimizing fracturing-flooding water injection parameters (Liu et al., 2024a; Zhu et al., 2024; Liu et al., 2024b; Lu et al., 2025; Yin et al., 2025).

Based on nonlinear flow, Biot's linear elasticity, and continuous damage theories, a fracturing-flooding mathematical model coupling hydro-mechanical-damage (H-M-D) for tight reservoirs was established in this study, integrated “fracturing-soaking-production” fracturing-flooding numerical simulation was performed, and the impact of different geological and engineering parameters on the fracturing-flooding effects were analyzed. Finally, the engineering parameters for fracturing flooding were optimized, and recommendations for field application were proposed.

2. Integrated “fracturing-soaking-production” fracturing-flooding mathematical model

The following assumptions are made for the rock and fluid during the water injection, soaking, and production processes: (1) Rock deformation follows Biot's linear elastic strain laws, and inertial forces are ignored. (2) The reservoir pores are saturated with oil and water phases, considered as 2D planar two-phase flow. (3) Salt solutes and oil displacement agents are only dissolved in the water phase, and instantaneous equilibrium is established between phases. (4) Reservoir fluids are incompressible Newtonian fluids, and the effect of gravity on fluid flow is ignored. (5) The effect of temperature on rock and fluid properties is ignored, and no physical or chemical reactions occur between the rock and fluid.

2.1. Hydraulic fracture propagation model

During the fracturing-flooding process, rock deformation includes both skeleton deformation (bulk deformation) and grain structure deformation (structural deformation). The momentum balance equation for rock deformation is as follows:

$$\nabla\sigma(u,p)+\rho_{\mathrm{b}}f=0 \tag{1}$$

where σ is the total stress of rock deformation, Pa; u is the displacement of rock deformation, m; p is the pressure on the rock, Pa; ρ_{b} is the rock density, kg·m^{-3}; f is the bulk force per unit volume of rock, m·s^{-2}.

Based on Biot's linear elastic stress theory (Cha et al., 2022), the constitutive relationship between fluid and matrix is established as follows:

$$\sigma=\sigma'-\alpha\cdot p_{\mathrm{m}} \tag{2}$$

where σ' is the effective stress of the rock, Pa; p_{m} is the pore fluid pressure in the rock, Pa; α is Biot coefficient, ranging from 0 to 1.

According to the effective stress and the stress-strain elastic relationship, the relationship between effective stress and rock displacement is obtained:

$$\sigma'=\lambda(\nabla\cdot u)+2G\varepsilon(u) \tag{3}$$

where ε is rock strain, dimensionless; λ is Lamé's first coefficient in continuum mechanics theory; G is Lamé's second coefficient in continuum mechanics theory.

The continuous damage model is used as the rock fracture initiation criterion, modeling a large number of localized microfractures caused by damage, while effectively predicting and adjusting fracture propagation direction in real-time based on the fracture index (Roth et al., 2015). By introducing the damage factor d, which represents the rock damage degree, the actual stress and effective stress of the formation are expressed as:

$$\sigma'=\frac{\sigma}{1-d} \tag{4}$$

where d is damage value of the rock element, dimensionless.

Based on the continuous damage model, the damage evolution function can be derived (Gunn, 1998):

$$d=1-\sqrt{\frac{r_0}{\overline{\varepsilon}}\exp\Big(-R_{\mathrm{f}}(\overline{\varepsilon}-r_0)\Big)} \tag{5}$$

where r_0 is ratio of tensile strength to elastic modulus, dimensionless; $\bar{\varepsilon}$ is average strain value of the rock, dimensionless.

R_f is the function related to the Young's modulus and tensile strength, which reflects the brittle characteristics of materials under tensile stress. Its expression is:

$$R_{\mathrm{f}}=\frac{2Ef_{\mathrm{t}}I_{\mathrm{rve}}}{2EG_{\mathrm{F}}-{f_t}^2I_{\mathrm{rve}}} \tag{6}$$

where E is the Young's modulus, MPa; f_t is the tensile strength, MPa; I_{rve} is the representative volume element characteristic length, dimensionless; G_F is the fracture energy, MPa.

In this model, the initiation and propagation of hydraulic fractures are controlled by a continuous damage model. When the stress state of the rock unit satisfies the damage evolution equation (Eq. (5)), damage begins to accumulate, marking the initiation of fractures. The propagation path of fractures is determined by the spatial distribution of the damage factor d. Therefore, the fracture network is a connected region composed of units where d is 1. Rock damage affects reservoir parameters such as porosity, permeability, and Young's modulus, expressed as:

$$\begin{cases} \phi_{\mathrm{d}}^0=\left(1-\phi^0\right)d^{\frac{3}{2}}+\phi^0 \\ k_{\mathrm{d}}^0=k^0\left(\dfrac{\phi_{\mathrm{d}}^0}{\phi^0}\right)^3 \\ E_{\mathrm{d}}^0=E^0(1-d)^2 \end{cases} \tag{7}$$

where ϕ^0 is the initial porosity, dimensionless; ϕ_d^0 is the damaged porosity, dimensionless; k^0 is the initial matrix permeability, mD; k_d^0 is the damaged matrix permeability, mD; E^0 is the initial Young's modulus, MPa; E_d^0 is the damaged Young's modulus, MPa.

2.2. Mathematical model for soaking imbibition

During the fracturing-flooding process, a large volume of injection water (either fresh water or river water) is introduced, with salinity generally ranging from 500 to 1000 mg/L. In contrast, the salinity of formation water can reach up to 1×10^5 mg/L, creating a significant salinity difference between the injected water and the formation water. Additionally, under the semi-permeable membrane effect of clay pores, osmotic pressure becomes a non-negligible factor in the underground fluid flow. This pressure is primarily determined by factors such as the chemical potential resulting from the salinity difference and the efficiency of the clay semi-permeable membrane (Mody and Hale, 1993). The expression for this is as follows:

$$p_\pi=\varepsilon_{\mathrm{n}}E_\pi RT\left(C_{\mathrm{r}}-C_{\mathrm{f}}\right) \tag{8}$$

where p_π is the osmotic pressure in clay pores, MPa; ε_n is the number of ions of salt solutes in the reservoir solution; R is the gas constant, 0.08206 (L·kPa)/(mol·K); T is the reservoir temperature, K; C_r is the molar concentration of salt solutes in formation water, mol/L; C_f is the molar concentration of salt solutes in injected fluid, mol/L.

Based on the theory of the double electric layer and combined with the Fritz's model (Fritz, 1986), the semi-permeable membrane efficiency E_π of clay minerals is characterized by parameters such as the solute concentration on both sides of the membrane, ion exchange capacity, clay mineral density, and porosity. The core samples of the target block were analyzed by X-ray diffraction, and the types and relative contents of its main clay minerals were determined. On this basis, the weighted average method was used to calculate the comprehensive membrane efficiency of mixed clay minerals.

$$E_\pi=1-\frac{(R_{\mathrm{ca-w}}+1)C_{\mathrm{a}}/C_{\mathrm{s}}}{\{R_{\mathrm{ca-w}}(C_{\mathrm{a}}/C_{\mathrm{c}})+1+R_{\mathrm{a-mw}}[R_{\mathrm{ca-m}}(C_{\mathrm{a}}/C_{\mathrm{c}})+1]\}\phi_{\mathrm{c}}} \tag{9}$$

where $R_{ca\text{-}w}$ is the ratio of friction coefficients between anions, cations in the solution and water; $R_{ca\text{-}m}$ is the ratio of friction coefficients between anions, cations in the solution and clay mineral membranes; $R_{a\text{-}mw}$ is the ratio of friction coefficients between anions in the solution and clay mineral membranes, water; C_a is the molar concentration of anions in the solution, mol/L; C_c is the molar concentration of cations in the solution, mol/L; C_s is the average molar concentration of salt solutes on both sides of the clay mineral, mol/L; ϕ_c is the porosity of clay minerals, %.

In formations containing multiple salt solutes, the complex multi-ion mixed solution is converted into an equivalent NaCl solution (Kurtoglu, 2013). The conversion formula is as follows:

$$C_{\mathrm{t}}=\sum_{i=1}^{n}\lambda_iC_i \tag{10}$$

where C_t is the total molar concentration of all ions in formation water, mol/L; C_i is the total molar concentration of the i-th ion in formation water, mol/L; n is the total number of ion types in formation water; i is the i-th ion species; λ_i is the conversion coefficient of the i-th ion in formation water.

This study selected 15 representative standard core columns from the research blocks, first saturated with formation water, and then injected simulated water with different ion compositions but known total mineralization. By measuring the potential difference between the two ends of the core during the seepage process and comparing it with the potential difference generated when injecting an equivalent NaCl solution, the electrochemical principles of Hittorf and Nernst Einstein were used for back calculation. Finally, the ion conversion coefficients λ_i applicable to the hydrochemical characteristics of the formation in this study block were obtained through weighted averaging, and the experimental standard deviation was controlled within ±5%.

During the imbibition process, capillary forces and osmotic pressure serve as the primary driving forces. Surfactant (oil displacement agent) plays a key role in the process of pressure flooding in tight reservoirs, including reducing oil-water interfacial tension, changing rock wettability, and further affecting capillary force. In addition, under the condition of a mineralization difference of 50000 mg/L, the osmotic pressure can reach 1–5 MPa. Therefore, the imbibition forces equation for low-permeability reservoirs can be expressed as:

$$\Delta p=p_c+p_\pi=\frac{2\sigma_{\mathrm{n}}\cos\theta}{r}+\varepsilon_{\mathrm{n}}E_\pi RT\left(C_{\mathrm{r}}-C_{\mathrm{f}}\right) \tag{11}$$

where Δp is the imbibition driving force, MPa; p_c is the capillary pressure, MPa; σ_n is the oil-water interfacial tension, MPa; θ is the rock wettability angle, °; r is the matrix pore radius, m.

The volume of imbibition between the matrix and fractures can be further derived as:

$$V_i = A\phi L_i = \frac{A\phi r}{4}\sqrt{\frac{1}{\mu}\left(\frac{4\sigma_{\rm n}\cos\theta}{r} + \varepsilon_{\rm n}E_{\pi}RT\left(C_{\rm r} - C_{\rm f}\right)\right)}\cdot\sqrt{t} \tag{12}$$

where V_i is the imbibition volume, m^3; L_i is the imbibition depth, m; A is the effective imbibition area, m^2; ϕ is the matrix porosity, %; μ is the fluid viscosity, mPa·s.

2.3. Mathematical model for oil and water flow

During fracturing-flooding process, oil displacement agents are co-injected with water, affecting fluid viscosity, interfacial tension, relative permeability, and rock wettability, thereby further improving oil displacement efficiency. Based on material balance, considering convection and diffusion, the mass conservation equation for each component is established:

$$\frac{\partial}{\partial t}(\phi\overline{C_i}) + {\rm div}\left(\overrightarrow{F}_i + \overrightarrow{D_i}\right) = Q_i \tag{13}$$

where $\overline{C_i}$ is the total concentration of component i in the pore volume; div is divergence, a quantity used to characterize the divergence degree of vector field in space; $\overrightarrow{F}_i$ is the convective volume of component i, m^3; $\overrightarrow{D_i}$ is the diffusion volume of component i, m^3; Q_i is the volume of component i flowing in or out per unit pore volume, m^3.

The convection equation is expressed as:

$$\overrightarrow{F}_i = \sum_{j=1}^{n_{\rm p}} \overrightarrow{V_j} C_{ij} \tag{14}$$

where $n_{\rm p}$ is the total number of phases in reservoir fluids, set to 2 (oil and water phases), dimensionless; V_j is the flow velocity of fluid phase j, m/s; C_{ij} is the volume fraction of component i in fluid phase j, dimensionless.

Based on the nonlinear flow model, ignoring gravity, the nonlinear flow coefficient is obtained through displacement experiments, and the low-velocity nonlinear flow motion equation is derived as follows:

$$\overrightarrow{V_j} = \frac{K\cdot K_{rj}}{\mu_j}\left(1 - \frac{m}{{\rm grad}\left(p_j\right) + m}\right){\rm grad}\left(p_j\right) \tag{15}$$

where K is the absolute permeability of the reservoir, mD; K_{rj} is the relative permeability of fluid phase j, dimensionless; μ_j is the viscosity of fluid phase j, mPa·s; grad (p_j) is the pressure gradient of fluid phase j, Pa/m; m is the low-velocity nonlinear flow coefficient, dimensionless.

The diffusion equation is expressed as:

$$\overrightarrow{D_i} = \sum_{j=1}^{n_{\rm p}} \phi S_j\left(\sum_{k=1}^{n_{\rm c}} D_{kj}^{i}\cdot{\rm grad}\left(C_{ij}\right)\right) \tag{16}$$

where S_j is the saturation of fluid phase j in the reservoir, dimensionless; $n_{\rm c}$ is the total number of components in fluid phase j, dimensionless; D_{kj}^{i} is the diffusion coefficient between component i and component k in fluid phase j, dimensionless.

The reservoir uses Dirichlet boundary conditions, with constant liquid injection and constant pressure production in the wellbore, and a fully closed unsteady no-flow outer boundary.

3. Solution and verification of the fracturing-flooding model

3.1. Solution of the mathematical fracturing-flooding model

In accordance with the practical engineering scenario of water injection during fracturing flooding, the injected water flows through the reservoir, causing changes in the rock stress field. These changes in the stress field induce rock damage, thereby, a coupled hydro-mechanical-damage (H-M-D) model can be established, as shown in Fig. 1. The model can be solved as follows: First, discretize the flow equation using the finite volume method (FVM) (Liu et al., 2025). Based on this, project and calculate the rock stress-strain field using the virtual element method (VEM). Finally, solve the flow-solid coupling problem using automatic differentiation (AD) to obtain the rock stress-strain parameters of the reservoir. Through the continuous damage model (CDM), the damage factor of each element can be calculated, and then the damage degree of each element can be determined. On this basis, the reservoir's rock mechanical parameters (effective stress, Young's modulus) and petrophysical parameters (porosity, permeability) can be corrected, which further influence the reservoir's flow field and stress-strain field.

3.2. Validation of two-phase flow model

This section omits the matrix-fracture imbibition model, the dynamic fracture propagation model, and the low-velocity nonlinear flow model in the current model. Using the Eclipse reservoir simulation software, a five-spot injection-production well pattern for oil-water two-phase flow is established to validate the two-phase oil-water flow model under waterflooding conditions presented in this paper. The Eclipse model adopts the same reservoir basic physical parameters (Table 1), relative permeability curve, and initial fluid saturation as this model.

As shown in Fig. 2, the Eclipse model treats the reservoir as an incompressible rigid body. During the early stage of water injection, the injection pressure rapidly rises to its maximum value. Later, as the pressure propagates and diffuses around the wellbore, the bottomhole pressure gradually decreases. The model in this

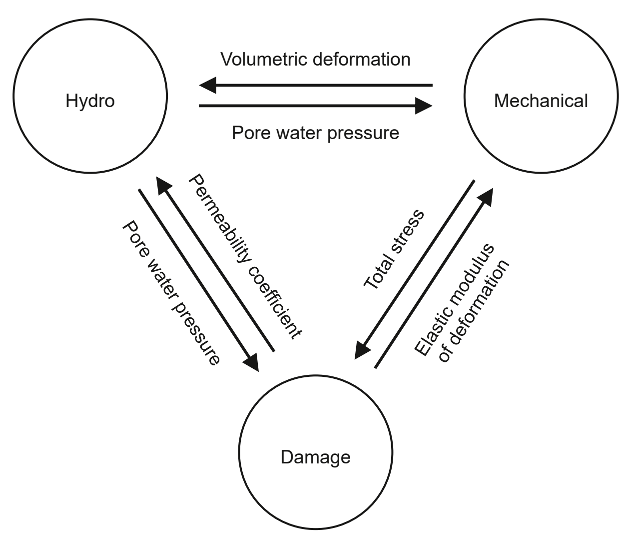

Fig. 1. Reservoir hydraulic-mechanical-damage diagram (H-M-D).

Table 1
Basic parameter settings of the reservoir.

Reservoir parameter	Value	Reservoir parameter	Value	Reservoir parameter	Value	Reservoir parameter	Value
Depth, m	3000	Crude oil compressibility, MPa^{-1}	6×10^{-4}	Direction of maximum horizontal principal stress, °	NE30°	Production well pressure, MPa	25
Reservoir pressure, MPa	35	Water compressibility, MPa^{-1}	4×10^{-4}	Horizontal principal stress difference, MPa	5	Production pressure difference, MPa	10
Matrix permeability, mD	5	Rock compressibility, MPa^{-1}	1×10^{-4}	Initial formation water salinity, mg/L	35000	Initial oil–water interfacial tension, mN/m	2
Matrix porosity, %	15	Initial oil saturation, %	60	Natural fracture length, m	75	Oil well spacing, m	400
Natural fracture permeability, mD	10000	Bound water saturation, %	30	Natural fracture density, fractures/m	0.01	Injection-production well spacing, m	283
Natural fracture porosity, %	60	Residual oil saturation, %	30	Natural fracture orientation, °	NE30°	Fracturing–flooding injection rate, m^3/d	1000
Crude oil viscosity, mPa·s	10	Young's modulus, MPa	3×10^4	Reservoir dimension, m	$808 \times 808 \times 40$	Fracturing-flooding injection volume, m^3	20000
Water viscosity, mPa·s	1	Poisson's Ratio	0.3	Reservoir grid blocks	$101 \times 101 \times 1$	Fracturing-flooding soaking duration, d	20
Crude oil density, kg/m	980	Matrix rock Biot coefficient	0.3	Injection water salinity, mg/L	1000	Conventional water injection rate, m^3/d	20
Water phase density, kg/m	1000	Natural fracture Biot coefficient	0.9	Injection surfactant concentration, %	0.2	Initial rock wettability angle, °	85

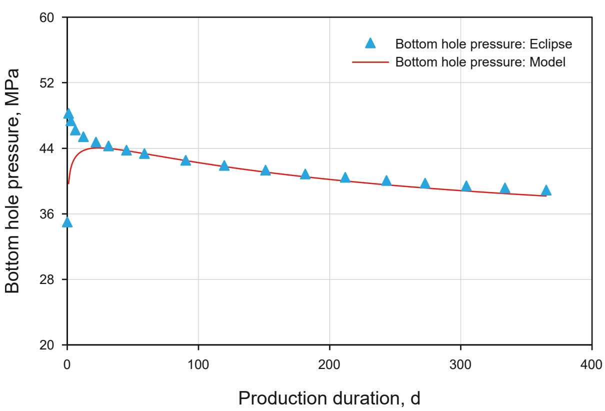

Fig. 2. Comparison of bottomhole pressure in injection wells.

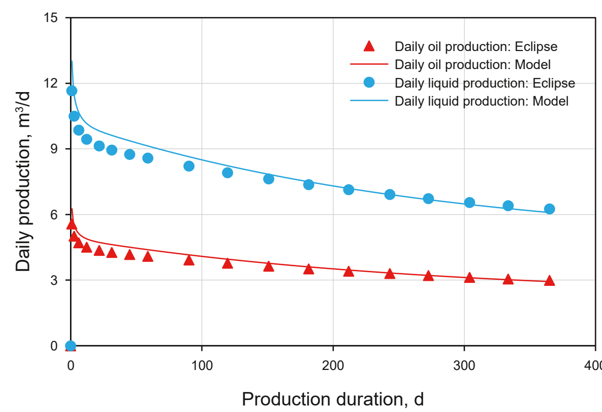

Fig. 3. Comparison of daily production for single wells.

paper considers the compressibility of the rock. During the early stage of water injection, as the bottomhole pressure increases, the rock deforms, the pore volume increases, and the rate of pressure rise in the reservoir slows down. This results in the bottomhole pressure at the injection well first rising to its maximum value, then gradually decreasing as the injection rate becomes lower than the pressure diffusion rate. When compared with field water injection data, it is shown that the model in this paper more accurately reflects the actual pressure changes in the formation during water injection.

For production wells, as shown in Fig. 3, after one year of production, the daily liquid production of a single well decreases from 12 m^3/d in the early stage to 6.1 m^3/d, and the daily oil production decreases from 6 m^3/d to 3.1 m^3/d. The error between the two models is less than 3%, confirming the accuracy of the basic flow model presented in this paper.

3.3. Validation of fracture propagation model

Based on microseismic fracture detection, it is shown that fracturing flooding often forms “long and narrow fractures”, with the fracture length much greater than the fracture height. Simplifying the dynamic fracture propagation model for fracturing flooding into a fracture propagation model for conventional hydraulic fracturing, the fracture propagation model for fracturing flooding can be then compared and validated with the classical PKN fracture propagation model.

As shown in Fig. 4, under the condition of water injection at 1000 m^3/d, after 1 h of fracturing flooding, the fracture length reaches approximately 42 m, with a fracture width of approximately 2.6 mm. The error with the PKN model is only 1.5%, indicating a high degree of agreement and validating the accuracy of the dynamic fracture propagation model presented in this paper.

4. Analysis of factors affecting fracturing-flooding effects

4.1. Basic fracturing-flooding parameter settings

As shown in Table 1, the simulated reservoir has a depth of 3000 m, an initial pressure of 35 MPa, and consists of oil-water two-phase fluid with a certain degree of natural fractures developed. The fracture orientation is consistent with the maximum horizontal principal stress, at an NE30° direction. The dimension of the simulated reservoir is 808 m × 808 m × 40 m, as shown in Fig. 5. To ensure the accuracy of numerical results and balance computational efficiency, this study conducted a grid sensitivity

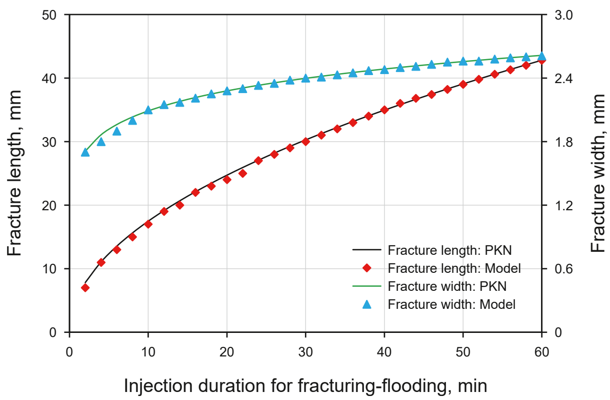

Fig. 4. Comparison of fracture propagation models.

analysis. Taking into account both computational accuracy and efficiency, the optimal grid division of 101 × 101 is reasonable and reliable. Taking the XX block as an example, for the fracturing-flooding water injection wells, the injection volume per cycle is set to 20,000 m^3, with an injection rate of 1000 m^3/d. The water injection is accompanied by the injection of a surfactant with an initial concentration of 0.2%. After the fracturing flooding ends, the soaking duration for the injection well (W1) is 30 days. Once the soaking period ends, the injection well transitions to conventional water injection with an injection rate of 20 m^3/d, and the oil well is produced at a constant pressure (set pressure to 25 MPa), with a production pressure differential of 10 MPa.

4.2. Analysis of the impacts of geological parameters

Field practice shows that natural fractures are an important factor affecting the waterflood front during fracturing flooding. Therefore, the geological parameters analyzed in this study include matrix permeability (0.1, 1.0, 5.0, 10 mD) and natural fracture density (0.5, 0.75, 1, 2 fractures/100 m).

4.2.1. Matrix permeability

As shown in Fig. 6, when the permeability is 0.1 mD, the formation filtration rate is low, the net pressure in the fractures is high, and the rock damage degree is high, resulting in “long and narrow” fracture zones (320 m long and 15 m wide). As matrix permeability increases (10 mD), the matrix filtration rate increases, making it easier to connect with natural fractures. As a result, the net pressure in the fracture network decreases, the rock damage degree decreases, and fracturing-flooding fractures are more influenced by natural fractures, forming “short and wide” fracture zones (216 m long, 41 m wide).

As shown in Table 2, when the matrix permeability is 0.1 mD, the matrix flow rate slows down, and the propagation velocity of the fluid pressure between matrix pores slows down too, resulting in a high-pressure zone near the injection well after fracturing-flooding water injection. During soaking period, the pressure diffusion rate is low, making it difficult for formation fluid pressure to diffuse. After 30 days of soaking, a distinct high-pressure zone persists in the formation, and pressure equilibrium is challenging to achieve. Even after three years of production, the formation pressure remains unbalanced. As matrix permeability increases, the flow rate within the matrix accelerates. Simultaneously, during water injection, hydraulic fractures connect with nearby natural fractures, enhancing the propagation velocity of fluid pressure within matrix pores. As a result, the high-pressure zone near the wellbore shrinks after fracturing flooding, and the formation fluid pressure diffuses more rapidly during the soaking period, gradually balancing the formation pressure. After soaking, the high-pressure zone significantly decreases, and the formation pressure drops at a faster rate during production.

4.2.2. Natural fracture density

As shown in Fig. 7, when the natural fracture density is low, it is more difficult for injected water to penetrate natural fractures. Therefore, the hydraulic fractures mainly extend in the direction of the maximum horizontal principal stress, with higher propagation pressure, resulting in longer hydraulic fractures and greater fracture damage. When the density of natural fractures increases from 0.5 to 2.0 fractures/100 m, the average deflection angle of the main branches of hydraulic fractures relative to the direction of the maximum horizontal principal stress (NE30°) increases from about 5° to about 15°. As the fracture density increases, the fracturing-flooding hydraulic fractures are more influenced by natural fractures, deviating and turning, forming shorter fracture networks with less damage.

As shown in Fig. 8, when the natural fracture density is 0.5 fractures/100 m, due to the underdeveloped fracture system in the reservoir, the fluid flow rate within the matrix and from the matrix to the fractures is slow, and the propagation velocity of the fluid

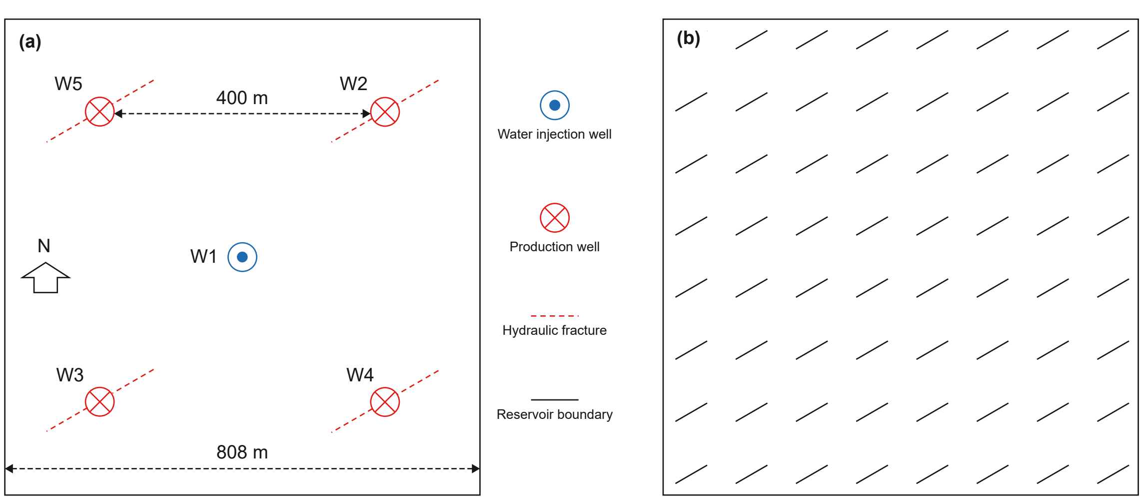

Fig. 5. Schematic diagram of the simulated injection-production well pattern. **(a)** Injection-production well group. **(b)** Natural fracture morphology.

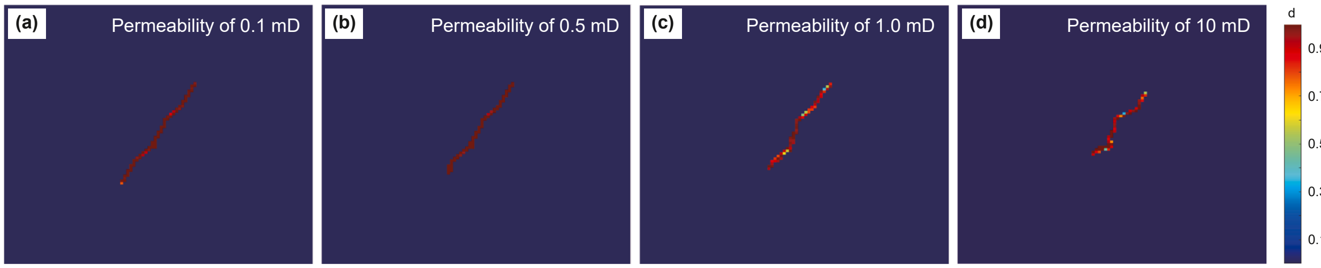

Fig. 6. Rock damage zones formed by fracturing-flooding under different matrix permeability conditions, the color represents the degree of damage to the rock unit, with red indicating high damage and blue indicating low damage. **(a)** Permeability of 0.1 mD. **(b)** Permeability of 0.5 mD. **(c)** Permeability of 1.0 mD. **(d)** Permeability of 10 mD.

Table 2
Numerical simulation of formation pressure distribution under different matrix permeability conditions, the colors represent formation pressure, with red indicating high pressure and blue indicating low pressure.

Matrix permeability	0.1 mD	1.0 mD	5.0 mD	10 mD
Formation pressure after water injection (20000 m^3)	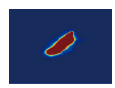	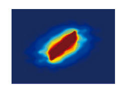	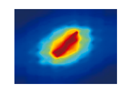	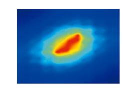
Formation pressure after soaking (20 d)	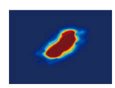	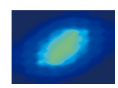		
Formation pressure after production (3 years)	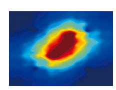	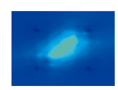		
Color bar	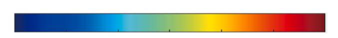			

pressure between pores is slow. After fracturing flooding, a high-pressure zone forms near the injection well. As the formation rock fractures, the bottom hole pressure gradually decreases from an initial 85 MPa to 75 MPa. During soaking period, the pressure diffusion velocity is relatively low, and the fluid pressure within the formation diffuses to some extent. After 30 days of soaking, the formation pressure near the injection well decreases from 75 MPa to 45 MPa, a drop of 30 MPa, but the formation pressure has not yet fully balanced. During three years of production, the formation pressure near the injection well gradually diffuses toward the production wells, and the overall formation pressure gradually decreases. As the natural fracture density increases, the flow distance from the matrix to the fractures becomes shorter, and the flow velocity increases. During water injection, hydraulic fractures easily connect with nearby natural fractures, increasing the propagation rate of the fluid pressure between matrix pores. After three years of production, the formation pressure in the reservoir with a low natural fracture density is about 29.5 MPa, and about 27.3 MPa in the reservoir with a high natural fracture density (1.0, 2.0 fractures/100 m), a decrease of 2.2 MPa.

4.3. Analysis of the impacts of engineering parameters

The impacts of engineering parameters on formation pressure, fracture propagation, water saturation, and later production during fracturing flooding is analyzed, and the engineering parameters includes fracturing-flooding water injection volumes of 5000, 10000, 20000, and 30000 m^3, water injection rates of 250, 500, 1000, and 1500 m^3/d, as well as soaking durations of 10, 20, 30, and 40 d.

4.3.1. Fracturing-flooding water injection volume

As shown in Figs. 9 and 10, when the water injection volume is 5000 m^3, during the early stages of injection, the formation fracture degree is low, and the formation pressure is high. The resulting fractures induced by water injection are short, with a

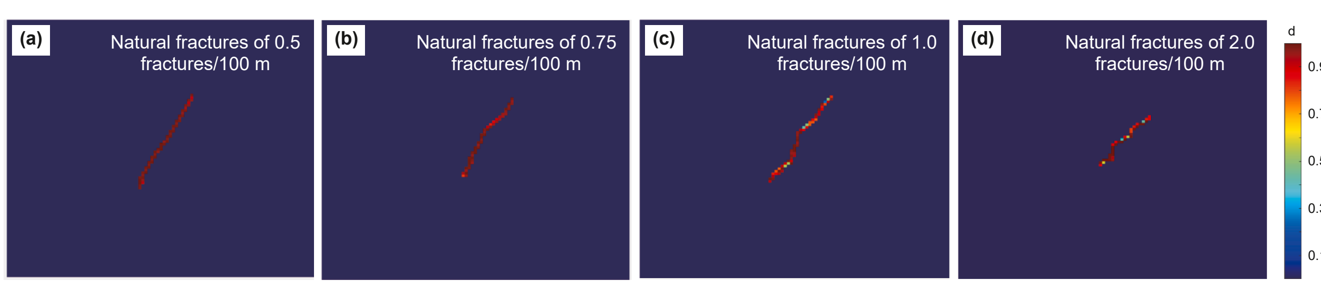

Fig. 7. Rock damage zones formed by fracturing-flooding water injection under different natural fracture densities, the color represents the degree of damage to the rock unit, with red indicating high damage and blue indicating low damage. **(a)** Natural fractures of 0.5 fractures/100 m. **(b)** Natural fractures of 0.75 fractures/100 m. **(c)** Natural fractures of 1.0 fractures/100 m. **(d)** Natural fractures of 2.0 fractures/100 m.

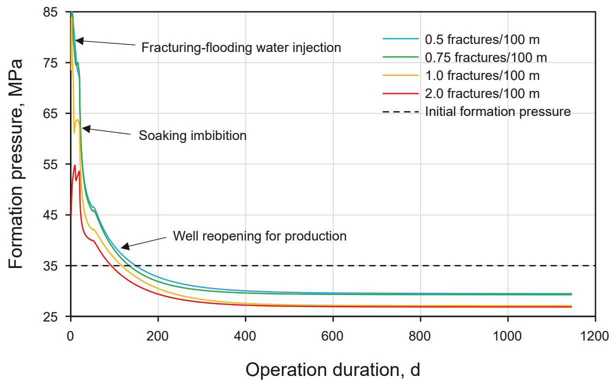

Fig. 8. Pressure changes during fracturing flooding under different natural fracture densities.

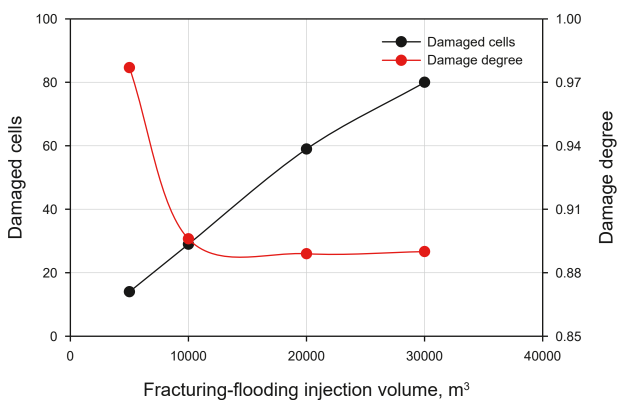

Fig. 9. The rock damage degree under different injection volumes of fracturing flooding.

length of approximately 85 m; however, the fracture damage is significant, with an average damage degree of 0.975. As the injection volume increases, the number of damaged cells rises, fracture length increases, and the overall water absorption capacity of the fracture network improves. Under the same injection volumes, formation pressure decreases. Therefore, in the later stages of fracturing flooding, newly formed hydraulic fractures (damaged cells) exhibit a lower damage level, with the average damage degree decreasing to 0.891. When the fracturing-flooding water injection volume within a single layer reaches 30000 m^3, the number of damaged cells increases to 80, with the length of fractures induced by water injection reaching 450 m. At this point, asymmetric fracture propagation occurs in the direction of the formation's principal stress. Influenced by natural fractures and formation stress heterogeneity, the hydraulic fractures are more likely to extend in the direction of stress dominance and may channel to the production wells, which is unfavorable for later conventional water injection and production.

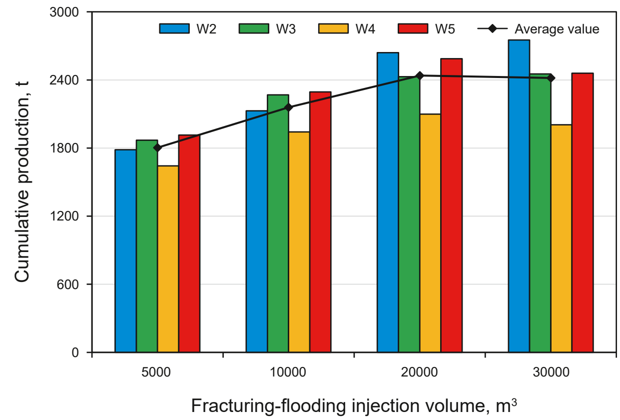

Fig. 11. Cumulative oil production of a single well under different injection volumes of fracturing-flooding.

As shown in Fig. 11, when the fracturing-flooding injection volume is 5000 m^3, the cumulative production of a single well is 1800 t. As the fracturing-flooding water injection volume increases, the formation energy in the early stages is more sufficient, resulting in a higher production rate after fracturing flooding and a greater cumulative production of a single well over three years. When the fracturing-flooding injection volume increases to 20000 m^3, the cumulative production of a single well increases to about 2400 t. Under these formation conditions, when the injection volume exceeds 20000 m^3, there is little increase in the production of the well group.

4.3.2. Fracturing-flooding injection rate

As shown in Figs. 12 and 13, when the injection rate is 250 m^3/d, the net pressure within the fractures is low, and the resulting hydraulic fractures have a low damage degree. The injection rate is small, comparable to the filtration rate of the formation fractures, and after fracturing flooding, the hydraulic fracture length is about 90 m. As the injection rate increases, the injection rate far exceeds the filtration rate of formation fractures, the number of damaged cells increases, the fracture length increases, and the formation net pressure increases, causing higher damage degree of the hydraulic fractures (damaged cells). When the injection rate increases to 450 m^3/d, the number of damaged cells increases to 104, and the hydraulic fracture length reaches a peak of 514 m. As the injection rate further increases, the net pressure within the fractures continues to increase, and the damage degree of the fracture cells

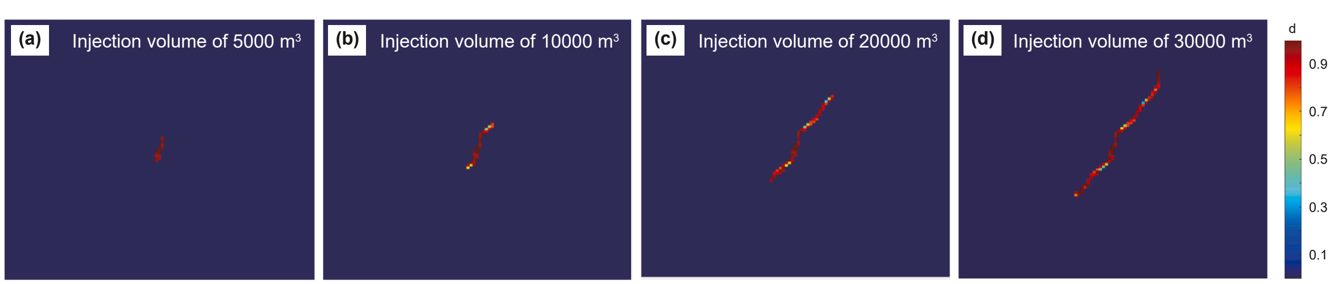

Fig. 10. Hydraulic fracture morphology formed under different injection volumes of fracturing flooding. **(a)** Injection volume of 5000 m^3. **(b)** Injection volume of 10000 m^3. **(c)** Injection volume of 20000 m^3. **(d)** Injection volume of 30000 m^3.

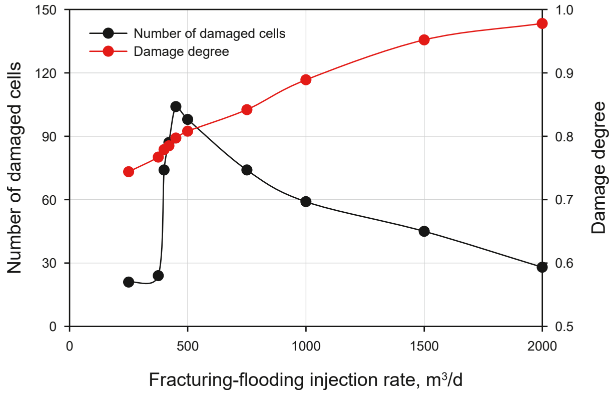

Fig. 12. The rock damage degree under different injection rates of fracturing-flooding.

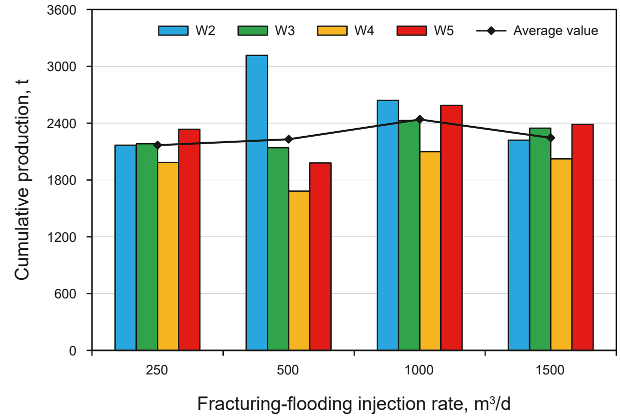

Fig. 14. 3-year cumulative oil production of a single well under different injection rates for fracturing flooding.

continues to increase. On one hand, as the net pressure within the fractures increases, the filtration rate within the fractures also increases. On the other hand, under the same injection volume, a higher injection rate results in a shorter injection duration and a shorter period of continuous damage to the formation. These two factors result in shorter hydraulic fracture lengths after fracturing flooding. Therefore, during fracturing-flooding water injection, considering the impact of formation net pressure and fracture filtration, it is necessary to control the fracturing-flooding injection rate to regulate the development of the fracture network, providing more suitable flow channels for later conventional water injection and production.

As shown in Fig. 14, the fracturing-flooding injection rate has a significant impact on cumulative production of a single well over three years. When the injection rate is 250 m^3/d, the cumulative production of a single well is about 1940 t. When the injection rate increases to 500 m^3/d, influenced by the hydraulic fractures, the cumulative production of Well W2 reaches 3200 t, while the cumulative production of other wells remains relatively low, with significant differences between wells. This disparity often leads to water channeling in the later stages of waterflooding or during the second-round fracturing-flooding process. Under the same fracturing-flooding injection volume, as the injection rate further increases, the hydraulic fracture length decreases, and the production wells are more evenly affected, consequently, the productivity of the wells improves to some extent.

4.3.3. *Fracturing-flooding soaking duration*

As shown in Fig. 15, the soaking duration has a significant impact on the formation pressure of the fracturing-flooding well group. As the soaking duration increases, the injected water near the injection well flows outward, and the pressure diffuses. After fracturing-flooding water injection of 20000 m^3, the formation pressure near the injection well increases to 64.2 MPa. After 10 days of soaking, the formation pressure decreases to 48.0 MPa, after 20 days to 44.8 MPa, and after 30 days to 43.5 MPa, gradually stabilizing. The stability of formation pressure is important for later balanced displacement and stable production. After 40 days of soaking, the formation pressure decreases to 42.8 MPa.

As shown in Fig. 16, when the soaking duration is 10 days, the cumulative production of a single well over three years is about 1920 t. When the soaking duration increases to 20 days, influenced by the formation pressure and oil saturation near the production wells, the cumulative production of a single well over three years increases to 2250 t. When the soaking duration increases to 30 days, the cumulative production of a single well over three years increases to 2430 t, and the cumulative production of the well group increases by 720 t. As the soaking duration further increases, the increase in cumulative oil production of the well group decreases.

5. Field application of fracturing flooding

Taking the fracturing flooding of tight oil reservoirs as an example, three fracturing-flooding well groups, G1, G2, and G3, were implemented. The fracturing-flooding parameters are shown in Table 3. For the G1 well group, the average single-stage injection volume ranges from 0.6 × 10^4 to 1.2 × 10^4 m^3, with an injection rate of 760 to 960 m^3/d and a soaking duration of approximately 70 days, characterized by the operational feature of “small injection volume and long soaking duration”. The G3 well group, in contrast, has an average single-stage injection volume of 3.7 × 10^4 to 4.2 × 10^4 m^3, with an injection rate of around 970 m^3/d and a soaking duration of 3 to 5 days, characterized by “large injection volume and short soaking duration”. The fracturing-flooding

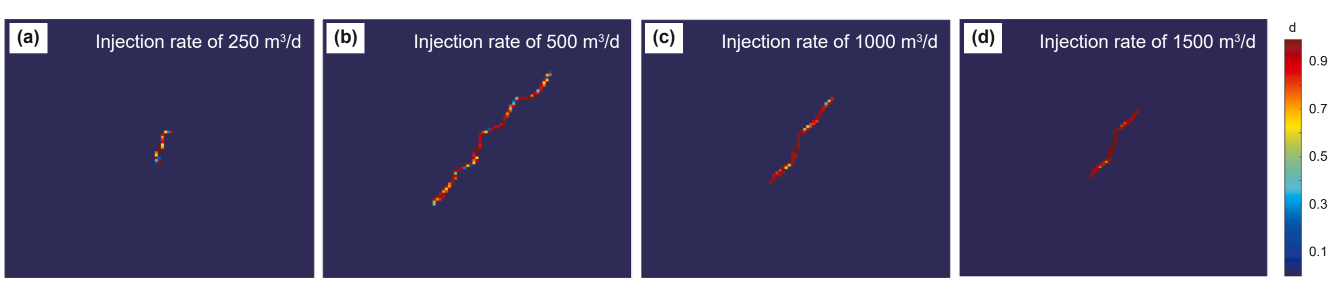

Fig. 13. Fracture morphology formed under different injection rates of fracturing-flooding. **(a)** Injection rate of 250 m^3/d. **(b)** Injection rate of 500 m^3/d. **(c)** Injection rate of 1000 m^3/d. **(d)** Injection rate of 1500 m^3/d.

Fig. 15. Rock damage zones formed by fracturing-flooding water injection under different natural fracture densities. **(a)** Soaking for 0 days. **(b)** Soaking for 10 days. **(c)** Soaking for 20 days. **(d)** Soaking for 30 days. **(e)** Soaking for 40 days.

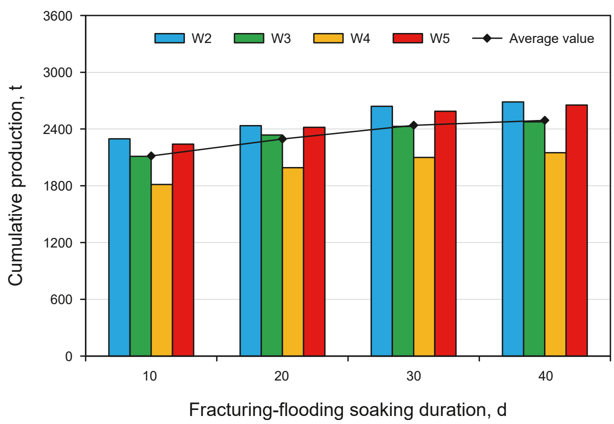

Fig. 16. Cumulative oil production of a single well over 3 years under different fracturing-flooding soaking durations.

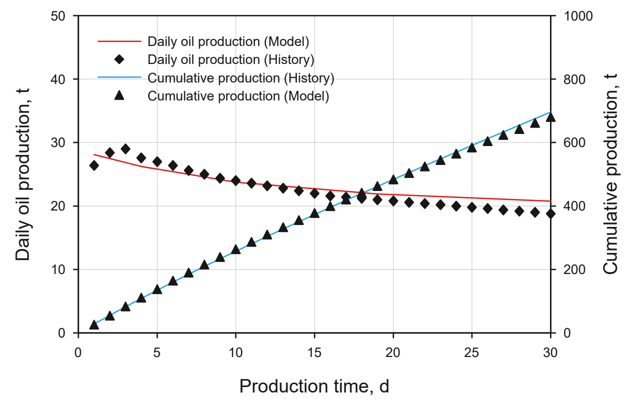

Fig. 17. Comparison between model and historical production data.

parameters for the G2 well group are roughly consistent with the values recommended by numerical simulation.

As shown in Fig. 17, by comparing and analyzing the numerical simulation results and historical production data of G2 well group, the daily oil production of the well group was 27.2 t/d at the initial stage, and the cumulative production was 696.3 t in a month, which was 2.2% higher than the numerical simulation results, further verifying the reliability of the research model.

The initial production results (1 month) of the well groups after fracturing flooding are shown in Table 4. Among them, the G2 well group shows the best production performance, while the G1 well group shows the characteristics of “low oil pressure, low liquid production, low oil production, and moderate water cut” after fracturing flooding. The main reason for this is that the G1 block has a small fracturing-flooding injection volume, resulting in insufficient energy replenishment and low liquid and oil production in later stages. Compared to the G2 well group, the G3 well group shows the characteristics of “moderate oil pressure, high liquid production, low oil production, and high water cut” after fracturing flooding. The reasons for this can be attributed to two factors: (1) Compared to the G2 block, the G3 block receives a larger fracturing-flooding injection volume, exceeding the formation's maximum water absorption capacity, resulting in water channeling in some production wells and sustained high water cut after well opening; (2) The soaking duration after fracturing flooding in the G3 block is too short, leading to insufficient diffusion of the injected water and weak oil-water imbibition. After reopening, the liquid production and the water cut from production wells is high, affecting the fracturing-flooding development effects. Based on the numerical simulation results, after 3 years of production, the oil production of G2 well group is 680–850 t higher than that of G1 and G3 well groups, and the economic benefits are

Table 3
Comparison of fracturing-flooding parameters for different well groups.

Well group	Well number	Injection volume, m^3	Injection rate, m^3/d	Soaking duration, d
G1	X1	12500	963.4	10
	X2	6100	763.1	70
	X3	7150	824.1	75
G2	X4	31812	1076.5	15
	X5	14136	648.8	15
G3	X6	36850	983.9	3
	X7	39850	973.0	5
	X8	41550	966.6	5
Numerical simulation recommended value		30000–35000	1000–1200	20–30

Table 4
Comparison of initial production performance after fracturing flooding in different well groups.

Well group	Average oil pressure, MPa	Average daily liquid production, t	Average daily oil production, t	Water cut, %
G1	0.5	13.0	5.5	35.6
G2	11.1	16.8	11.6	24.1
G3	11.6	31.5	4.4	64.0

much higher than the increase of G2 well group costs, including the additional costs of injection water, oil displacement agent and operation costs.

The optimization chart of fracturing-flooding engineering parameters obtained in this study is based on specific geological and engineering assumptions. When applied on site, it is necessary to comprehensively consider the specific geological uncertainty, construction constraints, and economic costs of the target block, and use real-time monitoring data for dynamic adjustment and adaptive management in order to achieve the best development effect.

6. Conclusions

(1) Considering the effects of capillary pressure and osmotic pressure, based on nonlinear flow theory and continuous damage theory, a coupled hydro-mechanical-damage (H-M-D) mathematical model for fracturing flooding in tight reservoirs was established. Numerical simulations of the integrated "fracturing-soaking-production" process were conducted to clarify the factors influencing-fracturing flooding effects.

(2) When matrix permeability is low, the formation's water absorption capacity is weak, and the rock damage degree is high, forming "long and narrow" fracture networks. As matrix permeability increases, the rock damage degree decreases, forming "short and wide" fracture networks. When natural fracture density is low, it is more difficult for injected water to penetrate natural fractures, resulting in longer hydraulic fracture networks and greater fracture damage during the fracturing-flooding process. As natural fracture density increases, the hydraulic fracture networks are more influenced by natural fractures, deviating and turning, forming shorter fracture networks.

(3) As the injected water volume increases, the length of the fracture network also increases, enhancing the overall water absorption capacity of the fracture network, and the hydraulic fractures are more likely to propagate in the direction of stress dominance. As the injection rate increases, the net pressure within the fractures rises, leading to greater fracture damage. As the soaking duration increases, the formation pressure equilibrates and diffuses, and under the influence of capillary and imbibition, the oil saturation near the fractures significantly increases after soaking.

(4) An integrated "fracturing-soaking-production" optimization technique for fracturing-flooding engineering parameters was formed, and an optimization chart for fracturing-flooding engineering parameters was established. The fracturing-flooding injection volume within a single layer was optimized to be 3.0×10^4 to 3.5×10^4 m^3, the fracturing-flooding injection rate was optimized to be 1,000 to 1,200 m^3/d, and the optimal soaking duration was optimized to be 20 to 30 days. These engineering parameters achieved better fracturing-flooding development results compared to adjacent blocks.

CRediT authorship contribution statement

Li Ma: Writing – review & editing, Writing – original draft, Validation, Software, Resources, Methodology, Investigation, Data curation, Conceptualization. **Jian-Chun Guo:** Supervision, Methodology, Jianfa Wu, Validation, Supervision, Methodology, Investigation. **Cong Lu:** Validation, Supervision, Methodology, Investigation, Funding acquisition. **Shi-Qian Xu:** Validation, Software, Methodology, Data curation. **Yi Song:** Data curation, Supervision, Writing – review & editing. **Cheng Shen:** Data curation, Software, Writing – original draft. **Jun-Feng Li:** Data curation, Project administration, Validation, Rui Yong, Resources, Methodology, Investigation.

Conflict of interest

We declare that we have no financial and personal relationships with other people or organizations that can inappropriately influence our work. There is no professional or other personal interest of any nature or kind in any product, service or company in the manuscript entitled "Numerical Simulation of Integrated 'Fracturing-Soaking-Production' in Tight Reservoirs".

Acknowledgements

This research was funded by the National Natural Science Foundation of China (Grant No. 52374044); the National Natural Science Foundation of China (Grant No. 52304045); Natural Science Foundation of Sichuan Province (Youth Science Fund Category B) (Grant No. 2026NSFSC1333).

References

Ahrenholz, B., Tölke, J., Lehmann, P., et al., 2008. Prediction of capillary hysteresis in a porous material using lattice-Boltzmann methods and comparison to experimental data and a morphological pore network model. Adv. Water Resour. 31 (9), 1151–1173. https://doi.org/10.1016/j.advwatres.2008.03.009.

Amico, S.C., Lekakou, C., 2004. Axial impregnation of a fiber bundle. Part 2: Theoretical analysis. Polym. Compos. 33 (2), 264–273. https://doi.org/10.1002/pc.10430.

Azeemuddin, M., Ghori, S.G., Saner, S., et al., 2002. Injection-induced hydraulic fracturing in a naturally fractured carbonate reservoir: A case study from Saudi Arabia. In: SPE International Symposium on Formation Damage Control. https://doi.org/10.2118/73784-MS.

Cai, X., Huang, Y., Jin, Z., 2023. Research and practice of pressure flooding in low-permeability reservoirs of complex fault block in Jiangsu Oilfield. Complex Hydrocarb. Reserv. 16 (3), 343–346. https://doi.org/10.16181/j.cnki.fzyqc.2023.03.016 (in Chinese).

Cha, L., Feng, Q., Wang, S., et al., 2022. Numerical simulation of fracture-flooding with virtual element method in a continuous damage model. Chin. J. Comput. Phys. 40 (1), 81–90. https://doi.org/10.19596/j.cnki.1001-246x.8538 (in Chinese).

Collins, P.M., 2007. Geomechanical effects on the SAGD process. SPE Res. Eval. Eng. 10 (4), 367–375. https://doi.org/10.2118/97905-PA.

Cui, C., Li, H., Wu, Z., et al., 2023a. Analysis of pressures in water injection wells considering fracture influence induced by pressure-drive water injection. Pet. Res. Eval. Dev. 13 (5), 686–694. https://doi.org/10.13809/j.cnki.cn32-1825/te.2023.05.016 (in Chinese).

Cui, C., Wang, J., Wu, Z., et al., 2023b. Establishment and application of pressure drive dynamic fracture model for tight oil reservoirs. Spec. Oil Gas Reserv. 30 (4), 87–95. https://doi.org/10.3969/j.issn.1006-6535.2023.04.011 (in Chinese).

Fritz, S.J., 1986. Ideality of clay membranes in osmotic processes: A review. Clays Clay Miner. 34 (2), 214–223. https://doi.org/10.1346/CCMN.1986.0340212.

Gao, T., Zhao, X., Dang, H., et al., 2018. Mechanism of cyclic water injection and its application in tight oil reservoirs in Yanchang Oilfield. Spec. Oil Gas Reserv. 25 (4), 134–137. https://doi.org/10.3969/j.issn.1006-6535.2018.04.027 (in Chinese).

Gunn, R.M., 1998. Non-linear analysis of arch dams including an anisotropic damage mechanics based constitutive model for concrete. Ph.D. Thesis, University of Brighton, Brighton, UK, pp. 56–78. https://www.researchgate.net/publication/33776065.

Guo, J., Ma, L., Lu, C., 2022. Progress and development directions of fracturing flooding technology for tight reservoirs in China. Acta Petrol. Sin. 43 (12), 1788–1797. https://doi.org/10.7623/syxb202212009 (in Chinese).

Hu, Y., Devegowda, D., Striolo, A., et al., 2015. Microscopic dynamics of water and hydrocarbon in shale-kerogen pores of potentially mixed wettability. SPE J. 20 (1), 112–124. https://doi.org/10.2118/167234-PA.

Hustedt, B., Snippe, J.R., 2010. Integrated data analysis and dynamic fracture modeling key to understanding complex waterfloods: Case study of the pierce field, North Sea. SPE Reserv. Eval. Eng. 13 (1), 82–94. https://doi.org/10.2118/132440-PA.

Kurtoglu, B., 2013. Integrated reservoir characterization and modeling in support of enhanced oil recovery for Bakken. Ph.D. Thesis, Colorado School of Mines, Colorado, US, pp. 28–36. https://doi.org/10.1145/2505515.2507830.

Li, G., Su, Y., Dong, Q., et al., 2022. Mathematical model of imbibition in porous media of fractured shale reservoir and its application. J. Cent. South Univ. Sci. Technol. (Nat. Sci. Ed.) 53 (9), 3301–3310. https://doi.org/10.11817/j.issn.1672-7207.2022.09.003 (in Chinese).

Li, K., Horne, R.N., 2001. Characterization of spontaneous water imbibition into gas-saturated rocks. SPE J. 6 (4), 375–384. https://doi.org/10.2118/74703-PA.

Li, K., Zhao, H., 2012. Fractal prediction model of spontaneous imbibition rate. Transp. Porous Media 91 (2), 363–376. https://doi.org/10.1007/s11242-011-9848-0.

Liu, C., Detournay, E., Zhang, F., 2024a. Finite domain solution of a KGD hydraulic fracture in the viscosity-dominated regime. Rock Mech. Bull. 3 (1). https://doi.org/10.1016/j.rockmb.2023.100095.

Liu, C., Zhang, F., Detournay, E., 2025. Finite domain solution of a hydraulic fracture in a permeable rock. Rock Mech. Bull. 4 (1), 100156. https://doi.org/10.1016/j.rockmb.2024.100156.

Liu, Y., Zhang, F., Weng, D., et al., 2024b. Two-phase flow thermo-hydro-mechanical modeling for a water flooding field case. Rock Mech. Bull. 3 (3), 100125. https://doi.org/10.1016/j.rockmb.2024.100125.

Lu, H., Qi, Y., Chen, W., et al., 2025. Coupling effect of temperature and confining pressure on fracture toughness of transversely isotropic shale: Insights from a thermal-mechanical DEM model. Rock Mech. Bull. 4 (4), 100211. https://doi.org/10.1016/j.rockmb.2025.100211.

Ma, Z., Shao, X., Li, G., et al., 2023. Application of dilatant pressure flooding technology in low permeability reservoir in Bonan Oilfield. Unconv. Oil Gas 10 (4), 58–66. https://doi.org/10.19901/j.fcgyq.2023.04.07 (in Chinese).

Mody, F.K., Hale, A.H., 1993. Borehole-stability model to couple the mechanics and chemistry of drilling-fluid shale interactions. J. Pet. Technol. 45 (11), 1093–1101. https://doi.org/10.2118/25728-PA.

Roth, S.R.S.H., Léger, P.P.L.P., Soulaïmani, A.A.S.E., 2015. A combined XFEM-damage mechanics approach for concrete crack propagation. Comput. Methods Appl. Mech. Eng. 283, 923–955. https://doi.org/10.1016/j.cma.2014.10.043.

Shen, Z., Wang, X., Kang, X., et al., 2018. Quantitative analysis of the mechanism of imbibition and displacement recovery of typical tight oil reservoirs in Yanchang Oilfield. Pet. Geol. Recovery Eff. 25 (5), 99–103. https://doi.org/10.13673/j.cnki.cn37-1359/te.2018.05.014 (in Chinese).

Shi, L., Cheng, S., Chang, Y., et al., 2022. Microscopic experiment and numerical simulation of spontaneous imbibition in tight oil reservoirs. J. China Univ. Pet. Nat. Sci.) 46 (1), 111–119. https://doi.org/10.3969/j.issn.1673-5005.2022.01.013 (in Chinese).

Wang, S., Feng, Q., Dong, Y., et al., 2015. A dynamic pore-scale network model for two-phase imbibition. J. Nat. Gas Sci. Eng. 26, 118–129. https://doi.org/10.1016/j.jngse.2015.06.005.

Wang, Y., Cheng, S., Zhang, K., et al., 2019. Pressure-transient analysis of water injectors considering the multiple closures of waterflood-induced fractures in tight reservoirs: Case studies in Changqing Oilfield, China. J. Pet. Sci. Eng. 172, 643–653. https://doi.org/10.1016/j.petrol.2018.07.052.

Xu, J., Liu, R., Liu, H., 2023. Optimization of shut-in time based on saturation rebalancing in volume-fractured tight oil reservoirs. Petrol. Explor. Dev. 50 (6), 1259–1267. https://doi.org/10.1016/S1876-3804(24)60478-7 (in Chinese).

Yang, Y., Zhang, S., Cao, X., et al., 2023. Practice and understanding of pressure drive development technology for low-permeability reservoirs in Shengli Oilfield. Pet. Geol. Recovery Eff. 30 (6), 61–71. https://doi.org/10.13673/j.pgre.202206036 (in Chinese).

Yin, Z., Zhang, Y., Zhang, F., et al., 2025. Dynamic evolution mechanisms of induced stresses in hydraulically fractured wells: Incorporating real gas characteristics. Int. J. Rock Mech. Min. Sci. 195, 106298. https://doi.org/10.1016/j.ijrmms.2025.106298.

Zhmud, B.V., Tiberg, F., Hallstensson, K., 2000. Dynamics of capillary rise. J. Colloid Interface Sci. 5 (2), 263–269. https://doi.org/10.1006/jcis.2000.6951.

Zhou, Y., 2017. Study on the micro-fracture propagation model by water-injection Induced in low permeability reservoirs. Ph.D. Thesis, China University of Petroleum (Beijing), Beijing, China, pp. 1–10 (in Chinese).

Zhu, H., Chen, S., Fu, Q., 2024. Geothermal extraction performance in fractured granite from Gonghe Basin, Qinghai province, China: Long-term injection and production experiment. Rock Mech. Bull. 3 (2), 100113. https://doi.org/10.1016/j.rockmb.2024.100113.